

Optical and electrical properties of InGaZnON thin films

Jian Ke Yao(姚建可), Fan Ye(叶凡), Ping Fan(范平)

Citation: Chin. Phys. B . 2020, 29(1): 018105 . **doi:** 10.1088/1674-1056/ab5fc1
Journal homepage: http://cpb.iphy.ac.cn; http://iopscience.iop.org/cpb

What follows is a list of articles you may be interested in

Excellent thermal stability and thermoelectric properties of *Pnma*-phase SnSe in middle temperature aerobic environment

Yu Tang(唐语), Decong Li(李德聪), Zhong Chen(陈钟), Shuping Deng(邓书平), Luqi Sun(孙璐琪), Wenting Liu(刘文婷), Lanxian Shen(申兰先), Shukang Deng(邓书康)

Chin. Phys. B . 2018, 27(11): 118105 . **doi:** 10.1088/1674-1056/27/11/118105

Raman spectroscopy characterization of two-dimensional materials

Fang Liang(梁芳), Hejun Xu(徐何军), Xing Wu(吴幸), Chaolun Wang(王超伦), Chen Luo(骆晨), Jian Zhang(张健)

Chin. Phys. B . 2018, 27(3): 037802 . **doi:** 10.1088/1674-1056/27/3/037802

Improved thermoelectric property of cation-substituted $CaMnO_3$

Pradeep Kumar, Subhash C. Kashyap, Vijay Kumar Sharma, H. C. Gupta

Chin. Phys. B . 2015, 24(9): 098101 . **doi:** 10.1088/1674-1056/24/9/098101

Influence of Ag and Sn incorporation in In_2S_3 thin films

Lin Ling-Yan, Yu Jin-Ling, Cheng Shu-Ying, Lu Pei-Min

Chin. Phys. B . 2015, 24(7): 078103 . **doi:** 10.1088/1674-1056/24/7/078103

Effects of the ion-beam voltage on the properties of the diamond-like carbon thin film prepared by ion-beam sputtering deposition

Sun Peng, Hu Ming, Zhang Feng, Ji Yi-Qin, Liu Hua-Song, Liu Dan-Dan, Leng Jian

Chin. Phys. B . 2015, 24(6): 067803 . **doi:** 10.1088/1674-1056/24/6/067803

Optical and electrical properties of InGaZnON thin films*

Jian Ke Yao(姚建可), Fan Ye(叶凡)†, and Ping Fan(范平)

Shenzhen Key Laboratory of Advanced Thin Films and Applications, College of Physics and Energy, Shenzhen University, Shenzhen 518060, *China*

(Received 29 August 2019; revised manuscript received 10 October 2019; accepted manuscript online 9 December 2019)

The substrate temperature (T_s) and N_2 partial pressure (P_{N2}) dependent optical and electrical properties of sputtered InGaZnON thin films are studied. With the increased T_s and P_{N2}, the thin film becomes more crystallized and nitrified. The Hall mobility, free carrier concentration (N_e), and electrical conductivity increase with the lowered interfacial potential barrier during crystal growing. The photoluminescence (PL) intensity decreases with the increased N_e. The band gap (E_g) narrows and the linear refractive index (n_1) increases with the increasing concentration of N in the thin films. The Stokes shift between the PL peak and absorption edge decreases with E_g. The n_1, dispersion energy, average oscillator wavelength, and oscillator length strength all increase with n_1. The single oscillator energy decreases with n_1. The nonlinear refractive index and third order optical susceptibility increase with n_1. The Seebeck coefficient, electron effective mass, mean free path, scattering time, and plasma energy are all N_e dependent.

Keywords: InGaZnON thin films, linear and nonlinear optical properties, Seebeck coefficient, electron effective mass

PACS: 81.05.Hd, 78.66.–w, 73.61.–r **DOI:** 10.1088/1674-1056/ab5fc1

1. Introduction

The InGaZnON (IGZON) thin films are now researched enormously as the active[1–3] or passivation[4] layers for thin film transistors to improve the stability.[5] The linear dispersive optical constants of IGZON thin films which are rarely studied till now are important to determine the sub-gap states in the thin films.[6–8] The structure of the crystalline IGZO thin film[9] is like that of the crystalline ZnO thin film which has non-centro symmetric structure with remarkable nonlinear optical response.[10,11] Generally, the third-order nonlinear optical susceptibility ($\chi^{(3)}$) and nonlinear refractive index (n_2) increase with linear refractive index (n_1).[12] The IGZO thin films have larger n_1 than the ZnO thin films,[8] indicating the better nonlinear optical response of the IGZO thin films. However, there are few experimental studies for the nonlinear optical properties of the IGZO thin films.[13] The nonlinear optical properties can also be theoretically investigated by the spectroscopy methods.[12,14,15] However, to our knowledge, there are none theoretical calculations done on the nonlinear optical properties of IGZO based thin films till now.

For accurate characterizing the electrical transport properties of the IGZON thin films, besides the free carrier concentration (N_e), Hall mobility (μ), and electrical conductivity (σ), the effective mass of free carriers (m_e^*)[16] and scattering time (τ)[17] should be determined together, but there are few related reports for the IGZON thin films. In this work, m_e^* and τ for the IGZON thin films are extracted using the Seebeck coefficients S.

The substrate temperatures (T_s)[8,18] and N_2 partial pressures (P_{N2})[1,7] during sputtering are crucial parameters determining the structure, composition, optical and electrical properties of thin films. Therefore, in this work, the T_s and P_{N2} dependent structure, composition, and optical and electrical properties of the IGZON thin films are investigated.

2. Experiment

The IGZON thin films were deposited by sputtering from an $InGaZnO_4$ target in diameter of 60 mm and thickness of 5 mm with the base pressure of 9.0×10^{-4} Pa and the working pressure of 0.5 Pa. The IGZON1 to IGZON3 thin films were grown under the conditions of $Ar : N_2 : O_2$ flow rates of 40 : 5 : 5 sccm, RF power of 200 W, and T_s of room temperature (RT), 300 °C, and 400 °C, respectively. And the IGZON4 to IGZON6 thin films were grown under the conditions of $Ar : N_2 : O_2$ flow rates of 40 : 10 : 0 sccm, RF power of 200 W, and T_s of RT, 300 °C, and 400 °C, respectively. All the thin films have the thickness of ∼ 350 nm.

The structures of the thin films were studied by a Rigaku x-ray diffraction (XRD) meter. Cu $K\alpha$ radiation at the wavelength of 0.15418 nm was used as the x-ray source. The surface morphologies of the thin films were studied by a ZEISS Gemini scanning electron microscope (SEM). The surface chemical states of the thin films were characterized by a Thermo ESCALAB 250 x-ray photoelectron spectrometer (XPS) with a mono-chromate Al $K\alpha$ x-ray source of energy 1486.6 eV and x-ray spot size of 500 μm. The test was taken at the chamber pressure of 10 mbar. The XPS spectra were collected under the condition with pass energy of

*Project supported by the National Natural Science Foundation of China (Grant No. 61674107), Shenzhen Key Lab Fund, China (Grant No. ZDSYS 20170228105421966), and Science and Technology Plan of Shenzhen, China (Grant No. JCYJ20170302150335518).

†Corresponding author. E-mail: yefan@szu.edu.cn

© 2020 Chinese Physical Society and IOP Publishing Ltd

20 eV and 0.05 eV/step for high-resolution scan. The low-energy electron flood gun with voltage of 3 V and current of 200 μA was applied to compensate the charging effects for the poor conductivity of the samples. The spectra were calibrated using the absorbed C 1s peak at 284.8 eV and fitted by Avantage software with Gaussian–Lorenzian curve with the shape of all peaks assumed to be 80% Gaussian and 20% Lorentzian. A smart mode was used to calculate the background. A Lambda 900 spectrometer was used to measure the transmittance of the thin films. To examine the defect states in the samples, the photoluminescence (PL, Edinburgh instrument, M300 Monochromator, Xe 900) spectroscopy was carried out at RT. To determine the optical constants and thickness of the thin films, the Spectroscopic ellipsometer (SE, Semilab GES5-E) was used. The carrier transportation properties and S of the thin films were obtained by a Hall system using the van der Pauw configuration (HMS 2000) and an S measuring apparatus (ZEM-3) at RT.

3. Results and discussion

The T_s during deposition is a crucial process parameter which can determine the growth of crystalline IGZO (C-IGZO) based thin films. The C-IGZO thin films usually appear at optimal T_s around 300 °C.[18] The IGZON thin films have minor N doping and therefore are still mainly IGZO based with similar texture and growth condition. Figure 1 and Table 1 show the XRD patterns and diffraction peaks parameters of the IGZON thin films. All thin films have the C-axis aligned crystal structure with (009) peak at 34°.[18] The (009) diffraction peak refers to $InGaZnO_4$ with hexagonal crystalline phase and R-3m (166) space-group with unit cell $3.295 \times 3.295 \times 26.07$ $\langle 90.0° \times 90.0° \times 120.0° \rangle$ referred from PDF#38-1104 crystallographic card. The (009) peak of the crystalline thin films indicates the high degree of crystallinity exhibited by domains oriented perpendicular to the substrate. These lattice planes correspond to the alternating layers of indium oxide and gallium/zinc oxide in the unit cell. The crystal grain size (G) of the thin films is calculated by $G = 0.89\lambda/(B\cos\theta)$, where λ is the wavelength of the x-ray (0.15418 nm), θ is the diffraction angle, and B is the full width at half-maximum of the crystal plane. The peak intensity and G slightly increase with T_s at both P_{N2}, indicating the growing of the thin film crystal. With the increase of T_s, the mobility of atoms adsorbed on the surface of the substrate increases, therefore the deposited thin film has improved crystalline and packing density. Figure 2 shows the surface morphologies of the thin films. All thin films have nano-crystalline structures. The grain size increases with the increased T_s and P_{N2} during deposition. The results are consistent with the XRD results in Fig. 1. The increased P_{N2} also increases G of the thin films as revealed by comparing IGZON4 to IGZON6 with IGZON1 to IGZON3 thin films.

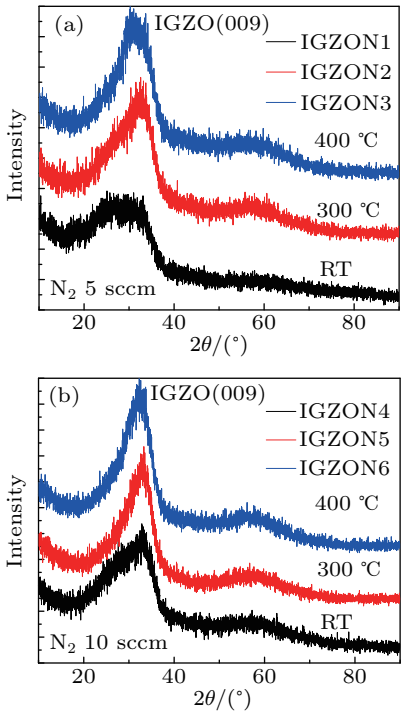


Fig. 1. XRD patterns of IGZON thin films deposited with increased T_s from RT to 400 °C at P_{N2} of (a) 10% and (b) 20%.

Table 1. The d, 2θ, B, and I of the IGZO (009) peaks and G of the IGZON thin films.

Samples	d-spacing/Å	$2\theta/(°)$	$B/(°)$	Peak intensity/arb. units	G/nm
IGZON1	2.6935	33.235	0.425	247	14.3
IGZON2	2.6885	33.299	0.288	318	28.5
IGZON3	2.7434	32.613	0.578	346	35.2
IGZON4	2.7161	32.950	0.121	238	38.1
IGZON5	2.6885	33.299	0.288	318	39.4
IGZON6	2.7434	32.613	0.578	346	40.1

The XPS spectra of O 1s and N 1s are shown in Fig. 3. The Gaussian fitting is used for fitting the combined O 1s peaks. The resulting sub-peaks at the binding energies of 530.3 eV, 530.9 eV, and 533.2 eV are attributed to O^{2-} surrounded by metal atoms, oxygen vacancies (V_O), and OH^{-1} impurities, respectively, at Figs. 3(a) and 3(b).[2] The signals of Ga Auger at 396.7 eV and Ga–N bonds at 397.8 eV are observed in Figs. 3(c) and 3(d).[2] The atomic ratios of V_O and N are calculated. It can be found that the concentration of V_O (C_{VO}, at.%) decreases with T_s at P_{N2} of 10% (Fig. 3(a)) due to the increased oxidation at higher T_s. At P_{N2} of 20% (Fig. 3(d)), with the increased T_s, the nitridation is slightly increased. With the concentration of N (C_N, at.%) slightly increased with the increase of T_s, C_{VO} also increases, which indicates the less oxidation than nitridation in the thin films, the less oxidation is also due to the oxygen escaping by the M–O bonds breaking during the deposition at higher temperature. The C_N slightly increases with T_s and P_{N2} by the increased nitridation at higher T_s and P_{N2}. At the same T_s, by comparing IGZON1 with IGZON4, IGZON2 with IGZON5, and IGZON3 with IGZON6, the thin films have larger C_N and C_{VO} by the slightly increased nitridation and decreased oxidation with the increased P_{N2}.

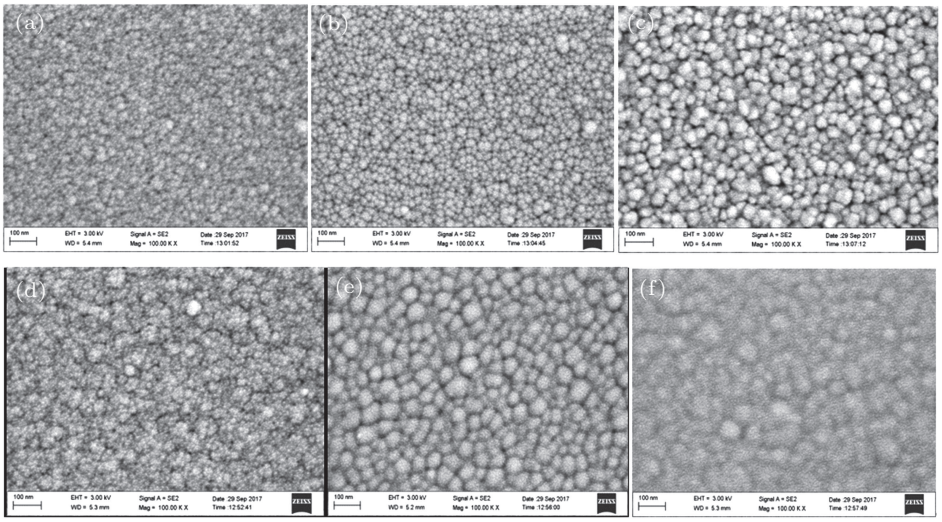


Fig. 2. The SEM surface morphologies with 10^5 magnification of the IGZON thin films deposited at (a) T_s of RT, P_{N2} of 10%; (b) T_s of 300 °C, P_{N2} of 10%; (c) T_s of 400 °C, P_{N2} of 10%; (d) T_s of RT, P_{N2} of 20%; (e) T_s of 300 °C, P_{N2} of 20%; (f) T_s of 400 °C, P_{N2} of 20%.

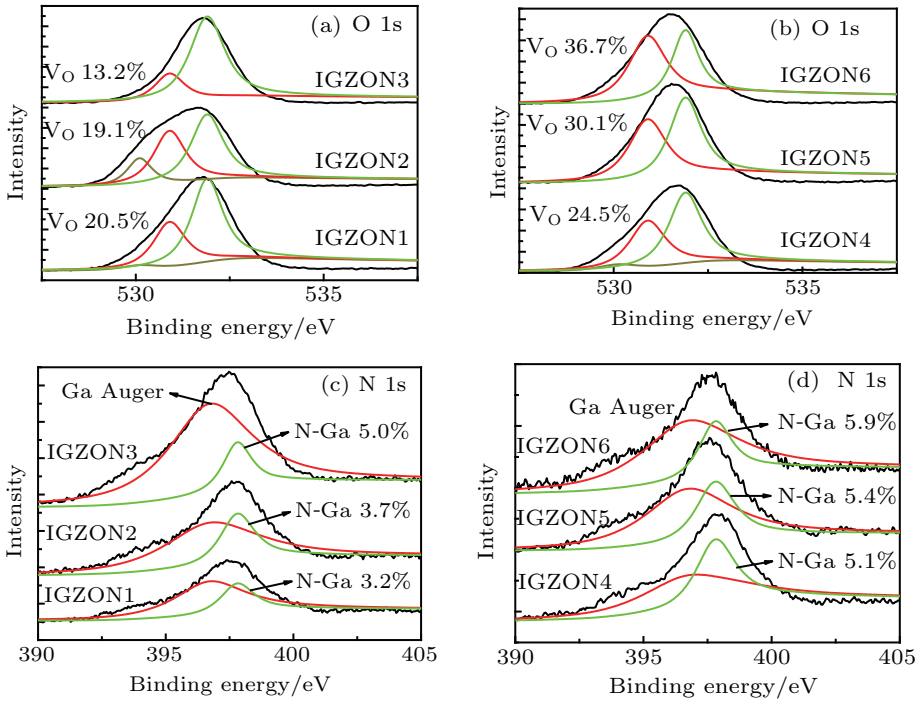


Fig. 3. The O 1s XPS spectra of IGZON thin films deposited at (a) P_{N2} of 10% and T_s of RT, 300 °C, and 400 °C; (b) P_{N2} of 20% and T_s of RT, 300 °C, and 400 °C. N 1s XPS spectra of IGZON thin films deposited at (c) P_{N2} of 10% and T_s of RT, 300 °C, and 400 °C; (d) P_{N2} of 20% and T_s of RT, 300 °C, and 400 °C.

The stokes shifts between the RTPL spectra excited by 325 nm laser and the absorption coefficients are shown in Fig. 4. The optical absorption coefficient α is defined as[19]

$$\alpha = -\frac{1}{d}\ln\left[\frac{T}{(1-R)^2}\right], \tag{1}$$

where T is the transmittance, R is the reflectance measured by the spectrometer as shown in Fig. 6, and d is the thickness of the thin film. The thin films exhibit broad and asymmetric PL spectra extended from UV to visible region with two peaks centered at 405 nm (3.06 eV) and 437 nm (2.84 eV).[20] The main violet emission peak centered at 3.06 eV is attributed to the electron transition from conduction band tail states to valence band tail states.[20] The minor blue emission at 2.84 eV is ascribed to the electron transition from interstitial to vacancy zincs. The PL intensity of the near-band-edge (NBE) emission strongly depends on the free carrier concentration (N_e) in the thin films. All IGZON thin films are n-type semiconductor. The N_e in the thin films increases with T_s and P_{N2} during deposition as seen in Fig. 5(a), which is due to the reduced crystal interfacial barriers with the increased size of the crystal grains in the thin films. As N_e increases, the PL intensity at 405 nm peak decreases. The PL and absorption spectra are compared. Between the two spectra, there exists a Stokes shift which is related to many effects such as electron–phonon coupling, lattice distortions, and interface and point defects.[21] The decrease of the Stokes shift as listed in Table 2 is ascribed

to the narrowing of the band gap (E_g) as seen later in Figs. 7(g) and 7(h).

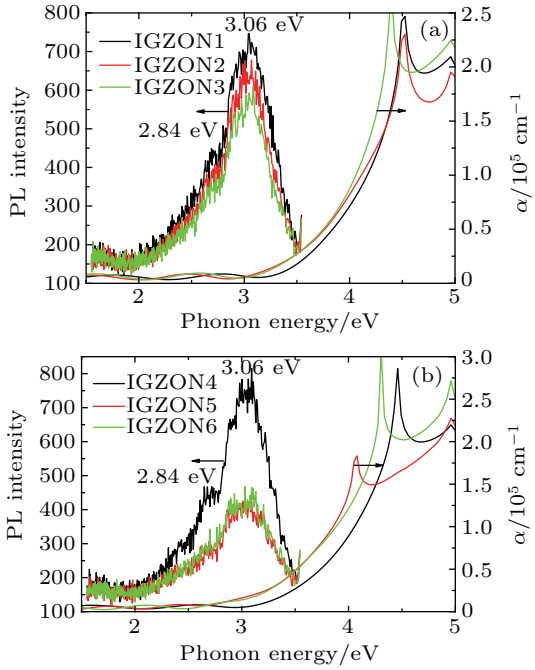


Fig. 4. The stokes shift between RTPL and absorption spectra for IGZON thin films deposited at T_s of RT, 300 °C, 400 °C and (a) P_{N2} of 10% or (b) P_{N2} of 20%.

The measured σ, μ, and S of the thin films are shown in Figs. 5(a) and 5(b). It is found that the T_s and P_{N2} have substantial influences on the charge transportation properties. The σ and μ increase with T_s and P_{N2} for the reduced interfacial crystal barrier by the increased crystalline size. The S depends on the temperature and electron effective mass (m_e^*) at the Fermi level and N_e as[22]

$$S = \frac{8\pi^2 k_B^2 T}{3qh^2} m_e^* \left(\frac{\pi}{3N_e}\right)^{2/3}, \tag{2}$$

where k_B is the Boltzmann constant, q is the electron charge, and h is the Plank constant. All thin films have negative S at RT, indicating the n-type conductivity. The S increases with N_e obeying well the relation (3), from which m_e^* can be calculated as shown in Fig. 5(b). For the IGZO thin film with N_e of 3.5×10^{20} cm^{-3}, the m_e^* is calculated to be 0.30 m_e^0, where m_e^0 is the static mass of electron.[23] The m_e^* increases with N_e for the non-parabolicity of the conduction band, which shows the validity of our result. For accurate characterizing the transportation properties, the free electron mean path (l_e) and scattering time (τ) are calculated by[24,25]

$$l_e = \frac{h}{2q}\left(\frac{3N_e}{\pi}\right)^{1/3}\mu, \tag{3}$$

$$\tau = \frac{m_e^*\mu}{q}, \tag{4}$$

where μ is the Hall mobility. The results are shown in Fig. 5(c). The smaller l_e than the crystal grain size in Table 1 indicates that the grain boundaries have no significant effects on the electrical transport properties. The l_e and τ are both N_e and μ co-dependent.

Figure 6 shows the transmittance and reflectance spectra of the IGZON thin films. All thin films are transparent in the visible region. The transmittance slightly decreases with T_s in the infrared region by free carrier absorption with the increased N_e.

The linear refractive index and dielectric constants are fitted by the SE method based on Cauchy and Drude models.[23] Figures 7(a) and 7(b) show that n_1 increases with T_s and P_{N2}. There are two mechanics for the increase of n_1. One is the increased crystal quality and packing density with the increased mobility of atoms adsorbed on the surface of the substrate at higher T_s. The other is the increased polarizability by N doping for the larger atomic radius of N than that of O.

The dispersion and absorption of dielectrics are represented by the empirical formula[26,27]

$$\varepsilon^* - \varepsilon_\infty = (\varepsilon_0 - \varepsilon_\infty)/[1 + (i\omega\tau_0)^{1-\alpha}], \tag{5}$$

where ε^* is the complex dielectric constant, ε_0 and ε_∞ are the static and high frequency dielectric constants, ω equals 2π times the frequency, and τ_0 is the generalized relaxation time. The parameter α can assume values between 0 and 1, the former giving the result of Debye for polar dielectrics. Figures 7(c) and 7(d) show the calculated real and imaginary dielectric constants (ε_1 and ε_2), that is the Cole–Cole plots, from which ε_∞ is determined at the interception of the real axis.

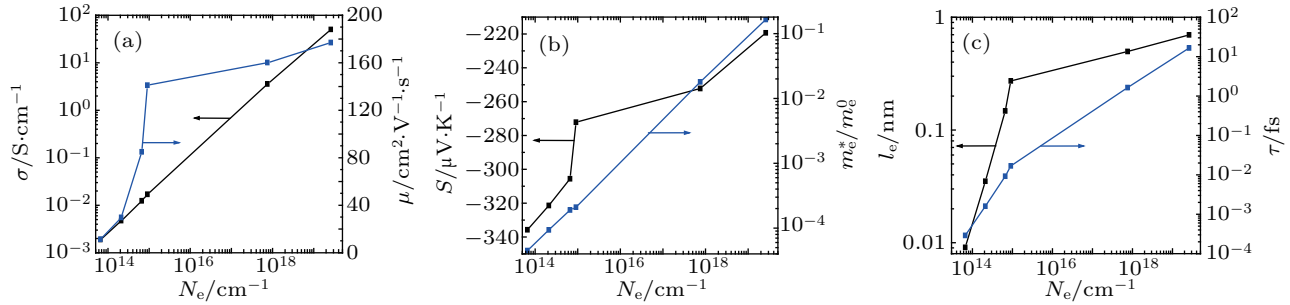


Fig. 5. The relation of (a) electrical conductivity (σ), Hall mobility (μ), (b) Seebeck coefficients (S), effective electron mass (m_e^*/m_e^0), (c) free electron mean path (l_e), and scattering time (τ) with N_e.

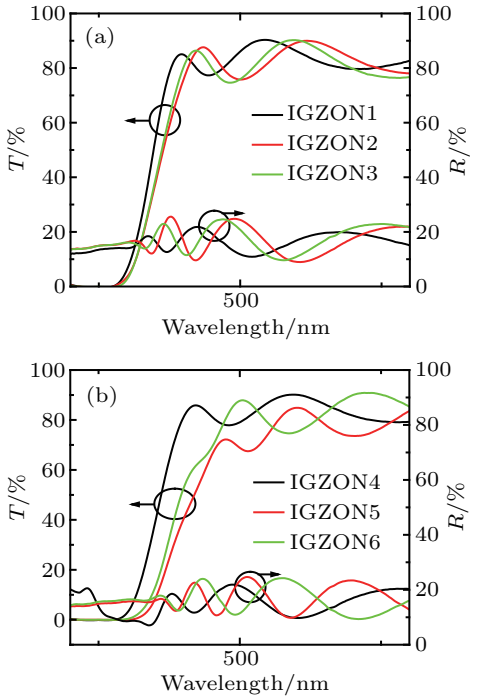


Fig. 6. The transmittance and reflectance spectra of IGZON thin films deposited at T_s of RT, 300 °C, 400 °C and (a) P_{N2} of 10% or (b) P_{N2} of 20%.

The onset of free carrier absorption is given by the plasma energy[28]

$$E_p = \left(\frac{h^2 q^2 N_e}{4\pi^2 m_e^* \varepsilon_\infty \varepsilon_0}\right)^{1/2}, \tag{6}$$

Figure 7(i) shows that E_p increases with N_e. It is known that the exponential optical energy dependence of α in the vicinity of the band gap can be described by[29]

$$\alpha \propto \exp\left(\frac{E}{E_u}\right), \tag{7}$$

where E is the photon energy and E_u is the Urbach energy related to the joint density of states determined by both conduction and valence band tail states. The extracted E_u is shown in Figs. 7(e) and 7(f). By assuming the parabolic densities of band states within IGZON, E_g is extracted by the Tauc method[30]

$$(E\alpha)^{1/2} = B(E - E_g), \tag{8}$$

where B is the slope. In Figs. 7(g) and 7(h), it is found that E_g is narrowed with the increase of T_s and P_{N2} during deposition for the IGZON thin films. The increases of T_s and P_{N2} during deposition have increased C_N in the IGZON thin films as seen in Figs. 3(c) and 3(d). As discussed by Ryu, with the increased C_N in thin films, the band gap decreases from 3.4 eV, 1.3 eV to 1.1 eV for ZnO, ZnON, and Zn_2N_3 thin films, respectively, which is mainly due to the N states in the valence band.[31] Therefore, in the IGZON thin films with the increase of C_N, E_g is narrowed. Although the free carrier concentration in the IGZON thin films is increased with the increase of T_s and P_{N2} during deposition as seen in Fig. 5(a). The band gap will widen with the increase of N_e due to the Burstein–Moss (BM) effect.[32] The electron–electron and electron–ion scatterings will also narrow the band gap. Here, the band gap narrowing by the increase of C_N in the thin films and by the electron–electron and electron–ion scatterings may be larger than the band gap widening by the BM effect. Therefore, for the IGZON thin films, with the increase of T_s and P_{N2} during deposition, E_g is narrowed.

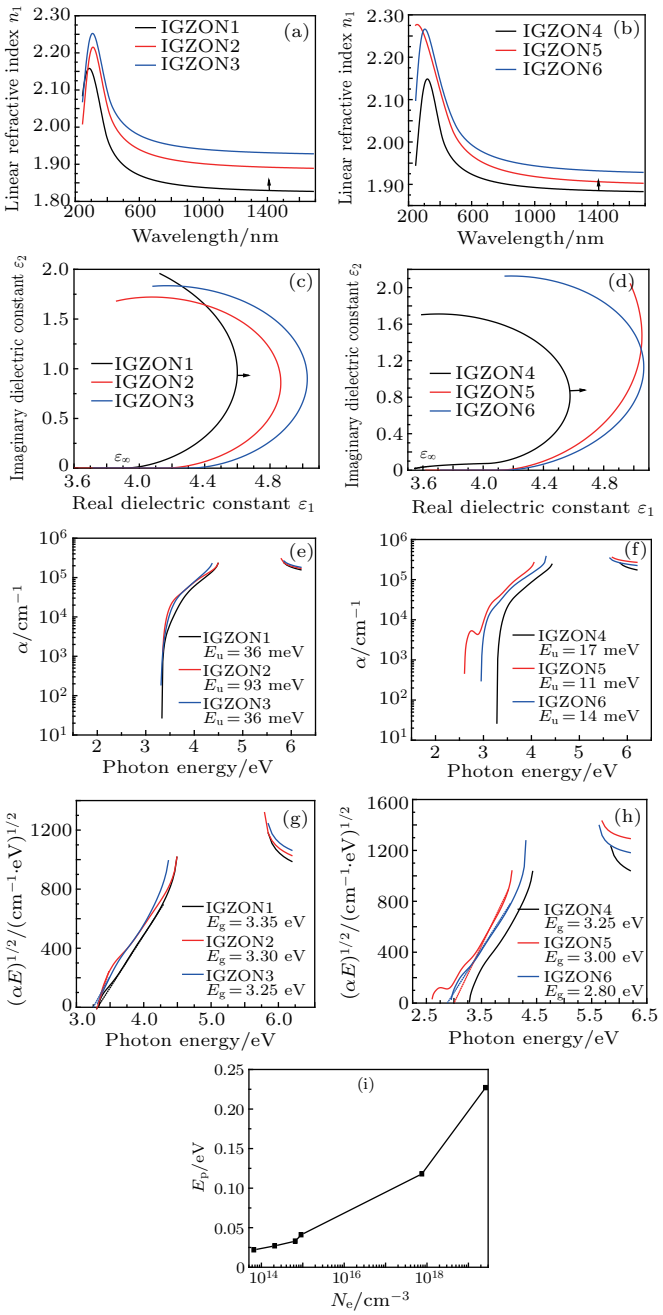


Fig. 7. (a), (b) Linear refractive index (n_1); (c), (d) Cole–Cole plots of dielectric functions; (e), (f) absorption coefficients (α); (g), (h) band gap (E_g); and (i) relation of plasma energy (E_p) with N_e for IGZON thin films.

The spectral dependent linear refractive index dispersion can be evaluated by the single-effective-oscillator model proposed by Wemple-Didomenico.[33] The n_1 of thin films can be

related with oscillator energy (E_o) and dispersion energy (E_d) by[33]

$$n_1^2 - 1 = \frac{E_o E_d}{E_o^2 - (h\nu)^2}, \tag{9}$$

where $h\nu$ is the photon energy, E_o and E_d are the single oscillator constants. E_o is the average excitation energy for electronic transitions and E_d is the dispersion energy which is a measure of the strength of inter-band optical transitions. This model describes the dielectric response for transitions below the optical gap. It plays an important role in determining the behavior of n_1. Figures 8(a) and 8(b) show the optical dispersion behavior of $(n_1^2-1)^{-1}$ vs. $(h\nu)^2$ for the IGZON thin films. The oscillator parameters E_o and E_d are determined by fitting a straight line to the points. The slope of the linear relation represents $(E_o E_d)^{-1}$ and the interception with the vertical axis equals to E_o/E_d. The increased values of E_o and E_d as listed in Table 2 indicate the improved structure order of the thin films with T_s and P_{N2}. The static refractive index n_s can be determined by[34]

$$n_s = (1 + E_d/E_o)^{1/2}. \tag{10}$$

Table 2. Optical and dispersion energy parameters for IGZON thin films.

Samples	1	2	3	4	5	6
Stokes shift/eV	1.6	1.5	1.5	1.5	1.3	1.1
E_o/eV	8.130	7.596	7.594	7.172	6.752	6.718
E_d/eV	16.679	17.541	18.249	19.476	20.524	20.582
λ_0/nm	4.8	4.8	4.9	4.9	5.1	5.3
S_0/nm^{-2}	0.10	0.10	0.11	0.11	0.12	0.14
n_s	1.824	1.879	1.889	1.900	1.924	1.924
ε_s	3.327	3.531	3.568	3.610	3.702	3.702
ε_∞	4.0	4.2	4.4	3.6	4.1	4.2

The static dielectric constant (ε_s) is estimated by $\varepsilon_s = n_s^2$.[33] It is observed that n_s and ε_s almost increase with T_s and P_{N2}. The refractive index can also be analyzed to determine the average oscillator wavelength (λ_0) and oscillator length strength (S_0) for the thin films. To obtain these values, the single term Sellmeier oscillator is used as[33]

$$n_1^2 - 1 = \frac{S_0 \lambda_0^2}{1 - \lambda_0^2/\lambda^2}. \tag{11}$$

The λ_0 and S_0 values are obtained by the linear parts of $1/(n_1^2-1)$ vs. λ^{-2} (not shown here), and the results are summarized in Table 2.

It is known that the induced dielectric polarization (P) depends on the applied electrical field (E) which can be expressed in a series of powers of E as[11]

$$P = \chi E + \chi^{(2)} E^2 + \chi^{(3)} E^3, \tag{12}$$

where $\chi^{(1)}$, $\chi^{(2)}$, and $\chi^{(3)}$ represent the linear, second, and third order nonlinear optical susceptibilities, respectively. The refractive index $n(\lambda)$ can be expressed as[11]

$$n(\lambda) = n_1(\lambda) + n_2(\lambda), \tag{13}$$

where $n_1(\lambda)$ and $n_2(\lambda)$ are the linear and nonlinear refractive indexes, respectively. The $\chi^{(1)}$ and $\chi^{(3)}$ are calculated by[11]

$$\chi^{(1)} = (n_1^2 - 1)/4\pi, \tag{14}$$

$$\chi^{(3)} = A[\chi^{(1)}]^4, \tag{15}$$

where A equals to 1.7×10^{-10} esu. The n_2 is calculated by[11]

$$n_2 = 12\pi\chi/n_1. \tag{16}$$

It is found that both the linear and nonlinear optical properties of the thin films enhance with T_s and P_{N2} during deposition. The $\chi^{(1)}$, $\chi^{(3)}$, and n_2 all increase and follow the same variation trend of $n_1(\lambda)$ for the improved crystalline and structural order and the increased C_N as seen in Figs. 8(c)–8(h).

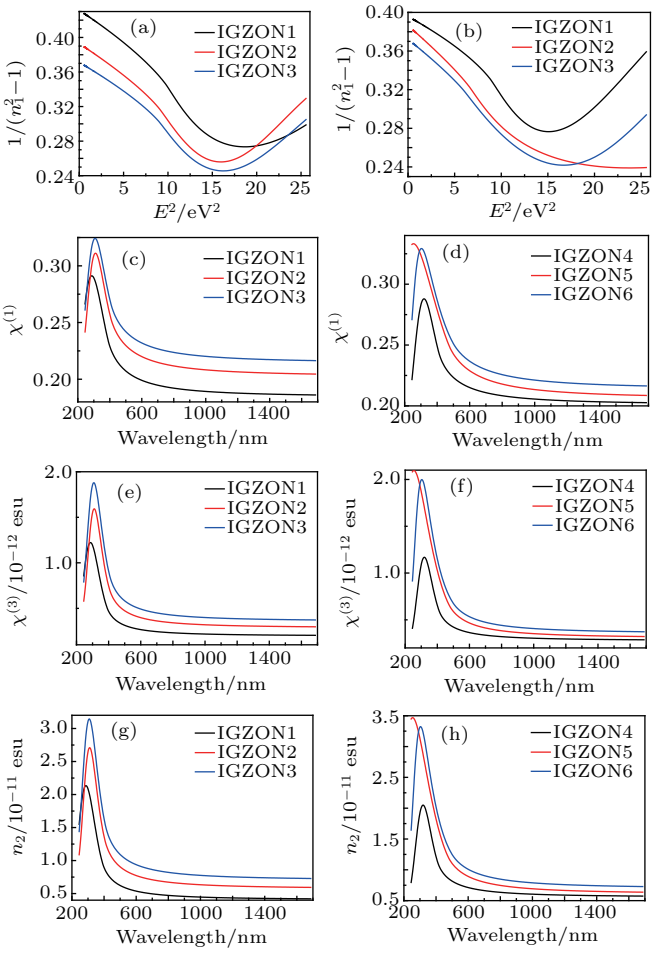


Fig. 8. The (a), (b) $(n^2-1)^{-1}$ vs. $(h\nu)^2$, (c), (d) $\chi^{(1)}$, (e), (f) $\chi^{(3)}$, and (g), (h) n_2 for IGZON thin films.

4. Conclusion and perspectives

The increase of T_s and P_{N2} during sputtering mainly enhances the crystallization which lowers the interfacial crystal potential barrier and therefore increases the μ, N_e, and σ of the IGZON thin films. The S, m_e^*, τ, l_e, and E_p are all increase with N_e. The increase of T_s and P_{N2} enhances the nitrification of the IGZON thin films. The n_1, n_2, $\chi^{(1)}$, and $\chi^{(3)}$ all increase with the improved crystallization and nitrification of the thin

films. The E_o decreases with the increase of n_1. The E_d, λ_0, and S_0 increase with the increase of n_1. The E_g narrows by the increased C_N which counteracts the widening effect by the increased N_e.

References

[1] Liu P T, Chang C H, Fuh C S and Sze S M 2016 *J. Disp. Technol.* **12** 1070

[2] Huang X M, Wu C F, Lu H, Ren F F, Chen D J, Zhang R and Zheng Y D 2013 *Appl. Phys. Lett.* **102** 193505

[3] Raja J, Jang K, Balaji N, Choi W, Trinh T T and Yi J S 2013 *Appl. Phys. Lett.* **102** 083505

[4] Liu P T, Chou Y T, Teng L F, Li F H, Fuh C S and Shieh H P D 2011 *IEEE Elec. Dev. Lett.* **32** 1397

[5] Kamiya T, Nomura K and Hosono H 2010 *Sci. Technol. Adv. Mater.* **11** 044305

[6] Kamiya T, Nomura K and Hosono H 2009 *J. Disp. Technol.* **5** 468

[7] Chen X, He G, Lv J, Liu M, Wang P, Chen X and Sun Z 2015 *J. Alloy. Compd.* **647** 1035

[8] Chen X F, He G, Gao J, Zhang J W, Xiao D Q, Jin P and Deng B 2015 *J. Alloy Compd.* **632** 533

[9] Yamazaki S, Koyama J, Yamamoto Y and Okamoto K 2012 *Society of Information Display Gigest* **183**

[10] Djuris A and Leung Y 2006 *Small* **2** 944

[11] Larciprete M and Centini M 2015 *Appl. Phys. Rev.* **2** 031302

[12] Malik G, Jaiswal J, Mourya S and Chandr R 2017 *J. Appl. Phys.* **122** 143105

[13] Sanal K, Vishnu K, Shijeesh M R and Jayaraj M K 2014 *Proc. SPIE* **9161** 91611B

[14] Shaaban E, El-Hagary M, Moustafa E, Hassan H, Ismail1 Y, EmamIsmail M and Ali A 2016 *Appl. Phys. A* **122** 20

[15] Jilani A, Abdel-wahab M, Zahran H, Yahia I and Al-Ghamdi A 2016 *Appl. Phys. A* **122** 862

[16] Wang Y Q, Zhu J H and Tang W 2014 *Appl. Phys. Lett.* **104** 212103

[17] Tang J, Deng L Y, Tay C B, Zhang X H, Chai J W, Qin H, Liu H W, Venkatesan T and Chua S J 2014 *J. Appl. Phys.* **115** 033111

[18] Lynch D, Zhu B, Levin B, Muller D, Ast D, Greene R and Thompson M 2014 *Appl. Phys. Lett.* **105** 262103

[19] Cai P G, Zhen D, Xu X J, Liu Y L, Chen N B, Wei G R and Sui C H 2010 *Mater. Sci. Eng. B* **171** 116

[20] Tiwari N, Chauhan R, Shieh H P D, Liu P T and Huang Y 2016 *IEEE Elec. Dev. Lett.* **63** 1578

[21] Sagara P, Shishodia P, Mehraa R, Okada H, Wakahara A and Yoshida A 2007 *J. Lumin.* **126** 800

[22] Korotcenkov G, Brinzari V and Ham M 2018 *Crystals* **8** 1

[23] Takagi A, Nomura K, Ohta H, Yanagi H, Kamiya T, Hirano M and Hosono H 2005 *Thin Solid Films* **486** 38

[24] Wang Y Q, Zhu J H and Tang W 2014 *Appl. Phys. Lett.* **104** 212103

[25] Tang J, Deng L Y, Tay C B, Zhang X H, Chai J W, Qin H, Liu H W, Venkatesan T and Chua S J 2014 *J. Appl. Phys.* **115** 033111

[26] Volintiru I, Creatore M and Sanden M 2008 *J. Appl. Phys.* **103** 033704

[27] Cole K S and Cole R H 1941 *J. Chem. Phys.* **9** 341

[28] Cole K S and Cole R H 1942 *J. Chem. Phys.* **10** 98

[29] Hamberg I and Granqvist C 1986 *J. Appl. Phys.* **60** R123

[30] Tharayila N, Sagarb S, Raveendrana R and Vaidyan A 2007 *Physica B* **399** 1

[31] Ryu M, Kim T S, Son K S, Kim H S, Park J S, Seon J B, Seo S J, Kim S J, Lee E, Lee H, Jeon S H, Han S and Lee S Y 2012 *IEEE International Electron Devices Meeting* **112**

[32] Hamberg I and Granqvist C 1986 *J. Appl. Phys.* **60** R123

[33] Fung T C, Chuang C S, Nomura K, Shieh H P D, Hosono H and Kanicki J 2008 *J. Inform. Disp.* **9** 21

[34] Yakuphanoglu F, Cukurovali A and Yilmaz I 2004 *Physica B* **351** 53